Synthesis, Crystal Structure and Magnetic Properties of K*Ln*Se_2 (*Ln* = La, Ce, Pr, Nd) Structures: A family of 2D Triangular Lattice Frustrated Magnets

Liurukara D. Sanjeewa,[a,b] Jie Xing,[c] Keith M. Taddei,[d] Athena S. Sefat[c]

[a]*Missouri Research Reactor, University of Missouri, Columbia, Missouri 65211, USA*
[b]*Department of Chemistry, University of Missouri, Columbia, MO 65211, USA*
[c]*Materials Science and Technology Division, Oak Ridge National Laboratory, Oak Ridge, Tennessee 37831, USA*
[d]*Neutron Scattering Division, Oak Ridge National Laboratory, Oak Ridge, Tennessee 37831, USA*

ABSTRACT

We report the detail synthesis, single crystal structure characterization and magnetic properties of K*Ln*Se_2 series obtained via solid state flux growth method. The crystal structures were characterized using single crystal x-ray diffraction. The K*Ln*Se_2 (*Ln* = La, Ce, Pr and Nd) series crystallizes in the trigonal crystal system with the space group of *R*-3*m* (No. 166). The overall structure contains two-dimensional (2D) layers made from edged shared *Ln*Se_6-octahedra. Ln^{3+} ions form a perfect triangular magnetic lattice which propagates along *ab*-plane. These triangular lattices are separated by the K^+ ions. The magnetic properties confirm that, Ce, Pr and Nd do not show any long-range ordering down to 0.4 K.

■ INTRODUCTION

The crystal structure and magnetic properties of the lanthanide-based oxides and intermetallics, which exhibit both geometrical spin frustration and competing magnetic interactions, have enticed materials chemists and physicists due to their potential for hosting complex magnetic and quantum ground states. [1-9] Quantum spin liquid (QSL), spin ice, and high temperature superconductivity are some of the exotic ground states of these materials which from the complex magnetic properties driven by the magnetic frustration. Over the last decade, special attention has been devoted in particular to the synthesis and characterization of novel QSL candidate materials focusing on two-dimensional magnetic sublattices such as triangular or kagomé in spin-1/2 systems to generate the necessary magnetic frustration prerequisite to the QSL state. Besides the rich exotic physics behind QSL s, QSL have been suggested as the basis for next generation technologies such as quantum computers and quantum communication . Additionally, understanding having confirmed QSL materials to study could allow new insights to the mechanism of high-temperature superconductivity. Therefore, the discovery and synthesis of new high quality QSLmaterials have received significant interest from the inorganic solid state and materials chemists. [10-20]

To these ends, Lanthanide intermetallic compounds with the formula of $ALnX_2$ (112-type compounds) where, A = Li, Na, K, Rb and Cs, Ln = Lanthanide, X = S, Se and Te have garnered growing interest from the community due to their exotic magnetic properties. [21-26] In these 112-type compounds the Lanthanide sites form triangular magnetic sub-lattices which due to the receptibility to numerous Ln members allow for a playground to study different magnetic interactions and spin-states on such a lattice. Special attention has been given to the Ce^{3+} [27-28] and Yb^{3+}-based [31-33] 112-type compounds due to their specific electron configuration, $4f^1$ and $4f^{13}$, respectively. These ions can produce the S = ½ spin state due to the crystal electric field and therefore host a QSL ground state(e.g. $YbMgGaO_4$, [29-30] $NaYbO_2$, [31] $NaYbS_2$ [32] and $CsYbSe_2$ [24-25, 33].) However, despite this focus on the Ce3+ and Yb3_ compounds, due to the variation in the number of unpaired electrons in the Ln^{3+}, 112-type compounds could exhibit wide variety of exotic magnetic ground states. For example, $KErSe_2$ [21] and $CsCeSe_2$ [34] tend to have a long-range AFM behavior at ~0.2 K with a stripe spin structure. Therefore, the ability to change the number of unpaired electrons in the Ln^{3+} allows for the stabilization of numerous different magnetic ground states in this series of compounds providing a route to study how different magnetic interactions and spin-states lead to different magnetic phases. On the other hand, the cation between the *Ln*-triangular layers could affect the dimensionality of the structure by tuning the inter-layer distance. This provides a second route to tune magnetic interactions in these materials with different magnetic grounds observed between compounds having different *A*-site cations. [24] However, despite this potential, only few examples of other *Ln*-based 112-type materials have been investigated so far, which could be due to the difficulty of synthesizing these materials in single crystal form. Recently we have developed a very successful flux growth technique to get good sizable single crystals of 122-type compounds. [24] Therefore, we extend our work to synthesize K-based early lanthanides (La, Ce, Pr and Nd) and study their magnetic properties.

Herein, we report the synthesis and magnetic properties of $KLnSe_2$, *Ln* = La, Ce, Pr and Nd series. Single crystals of $KLnSe_2$ series were grown successfully using our previously reported flux growth method. These compoundscrystallize in trigonal symmetry with *R*-3*m* space group where Ln^{3+} ions form a perfect triangular lattice. The magnetic properties were characterized in the form of *dc*-magnetic susceptibility, and heat capacity down to 0.4 K.

■ EXPERIMENTAL SECTION

Reagents. K (Alfa Aesar, 99.95%), La-rod (Alfa Aesar, 99.9), Ce-rod (Alfa Aesar, 99.8%), Pr-rod (Alfa Aesar, 99.1%), Nd-rod (Alfa Aesar, 99.5%) and Se-shots (Alfa Aesar, 99.999%) were all used as received.

Synthesis. Crystal growth was performed using a two-step method. As the first step, powder samples were synthesized using the constituent elements. As the second step, the powder samples were mixed with the salt flux to grow single crystals. In a typical reaction, a total of 2 g of K, *Ln* and Se were loaded into an alumina crucible. Here, all the chemicals were handled inside the glove box with the oxygen and water levels as < 0.1 ppm level. Potassium is extremely reactive in air (being pyrophoric,) therefore extra precaution is necessary to avoid any contact with O_2 or H_2O. After loading all the components into an alumina(?) crucible, it was inserted into a quartz tube and sealed inside the glove box using a swagelok. Then the quartz tubes were evacuated and sealed on a sealing line. The fused-silica ampoules were then heated to 100 °C at 5 °C/hr and held for one day, heated to 600 °C 10 °C/hr and held for two days followed by slowly cooling to room temperature. After the reaction period, the sealed tubes were opened, and powders were recovered inside the glove box. 1 g of the powder was then loaded into a quartz tube with 10 g of dried KCl (1: 10 flux ratio by weight) and the reactions were evacuated and sealed. The sealed tubes were heated to 800 °C at 60 °C/hr and kept for 2 weeks. After the reaction period, the reactions were quenched in open air. The crystals were recovered by washing with deionized water using the suction filtration method.

Single-Crystal X-Ray Diffraction. X-ray single-crystal diffraction (SXRD) data were collected using Bruker Quest D8 single-crystal X-ray diffractometer equipped with Mo Kα radiation, λ = 0.71073 Å. The data were collected at room temperature and crystals were mounted in paratone oil. The crystal diffraction images were collected using ϕ and ω-scans. The diffractometer was equipped with an Incoatec IμS source using the APEXIII software suite for data setup, collection, and processing. [35] Structure refinements was done using the SHELXTL software suite. [36] Table 1 provides the detailed unit cell parameters of $KLnSe_2$ series and the selected bond distances are summarized in Table 2. Details regarding the X-ray powder diffraction (PXRD) and elemental analysis are given under the Supporting Information.

The magnetic properties were measured using a Quantum Design (QD) Magnetic Properties Measurement System (MPMS3). First, the magnetic properties between 2-300 K were determine using the single crystals. The anisotropic magnetic properties were measured by applying the magnetic field parallel and perpendicular to the *Ln*-triangular magnetic lattices. The weight of the crystals was 3-8 mg. The magnetic properties below 2 K was measured using the MPMS3 iHe3 option. Heat capacity measurements were also performed using the single crystals. Here, heat capacity was measured using QD Physical Properties Measurement System (PPMS). The mass of the single crystals for heat capacity was ~1 mg.

Table 1. Crystallographic data of $KLnSe_2$ (*Ln* = La, Pr, Ce and Nd) determined by single-crystal X-ray diffraction.

empirical formula	$KLaSe_2$	$KCeSe_2$	$KPrSe_2$	$KNdSe_2$
formula weight (g/mol)	335.93	337.14	337.93	341.26
T, K	300	300	300	300
Crystal habitat	clear, plate	red plates	green plates	red plates
Crystal dimensions, mm	0.06 × 0.02 × 0.02	0.08 × 0.01 × 0.01	0.06 × 0.01 × 0.01	0.08 x 0.01 x 0.01
crystal system	trigonal			
space group	*R-3m* (No.166)			
a, Å	4.4048(1)	4.3680(1)	4.3287(5)	4.3134(2)
c, Å	22.785(1)	22.7761(6)	22.752(5)	22.793(3)
volume, $Å^3$	382.9(3)	376.34(2)	369.21(2)	367.2(3)
Z	3	3	3	3
D (calc), g/cm^3)	4.371	4.463	4.560	4.629
μ (Mo Kα), mm^{-1}	23.249	24.210	25.327	26.118
F(000)	432	435	438	441
Tmax, Tmin	0.3360/0.4410	0.2480/0.7940	0.0071/0.0325	0.0052/0.0325
θ range	2.68-30.43	2.68-30.46	2.69/30.58	2.68-30.64
reflections collected	2420	5023	2452	1088
data/restraints/parameters	117/0/8	115/0/8	111/0/8	110/0/8
final R [I> 2σ(I)] R_1, R_{w2}	0.0196/0.0436	0.0141/0.0351	0.0402/0.0872	0.0226/0.0539
final R (all data) R_1, R_{w2}	0.0211/0.0448	0.0167/0.0401	0.0453/0.0914	0.0246/0.0556
GoF	1.088	1.062	1.062	1.070
largest diff. peak/hole, e/ $Å^3$	0.515/-0.624/0.154	0.527/-0.578/0.137	3.278/-1.856/0.318	0.781/-0.879/0.194

Table 2. The selected bond distances (Å) and angles (°) of $KRESe_2$ (*RE* = La, Ce, Pr and Nd) series.

	$KLaSe_2$	$KPrSe_2$	$KPrSe_2$	$KNdSe_2$

RE–*RE*	4.4048(1)	4.3680(1)	4.3287(5)	4.3134(2)
RE–Se–*RE*	93.58(3)	93.59(7)	93.42(6)	93.43(4)
Interlayer *RE*–*RE*	7.595	7.562	7.584	7.597

■ RESULTS AND DISCUSSION

Crystal Structure. At room temperature, all K*Ln*Se_2 compounds crystalize in a trigonal crystal system with space group of *R*-3*m* (No. 166). The detailed crystallographic information is presented in Table 1. The unit cell parameters are follows: for $KLaSe_2$, *a* = 4.4048(1) Å, *c* = 22.785(1) Å, *V* = 382.9(3) Å^3, for $KCeSe_2$, *a* = 4.3680(1) Å, *c* = 22.7761(6) Å, *V* = 376.34(2) Å^3, for $KPrSe_2$, *a* = 4.3287(5) Å, *c* = 22.752(5) Å, *V* = 369.21(2) Å^3, and for $KNdSe_2$, *a* = 4.3131(2) Å, *c* = 22.793(3) Å, *V* = 367.2(3) Å^3. The structure is built from a single unique Wyckoff site for each ion with K^+ (3*b*), Ln^{3+} (3*a*) and Se^{2-} (6*c*). The Ln^{3+} and Se^{2-} ions form 2D La–Se–La layers where the K^+ ions reside in between the layers. Figure1a shows the overall structure of $KLaSe_2$. The 2D layers of $KLaSe_2$ are constructed from edge sharing $LaSe_6$-octahedra. The La^{3+} 2D layers are shown in Figure 1b. It is noteworthy to point out that, all the studied K*Ln*Se_2 (La- Lu) series compounds crystallize in the *R*-3*m* space group - we did not observe any structural changes with the change of size of the lanthanide ions. This is somehwat diffrent from the Cs*Ln*Se_2 series where smaller lanthanides crystallize in $P6_3/mmc$. The La- site forms $LaSe_6$-octahedra (Figure 1c) which share edges with each other to form the La–Se–La 2D layers. In these structures, the interlayer distance

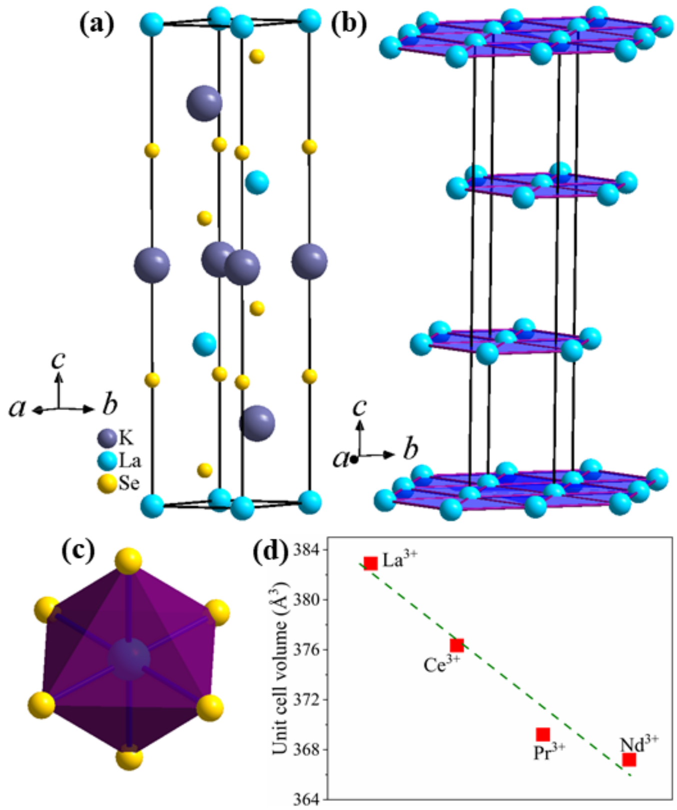

is mainly controlled by the size of the *A*-site cation which is K^+ in this case. Therefore, we observed a minimum change of the interlayer distances between the structures. However, since the size of the Ln^{3+} ion changes from La to Nd, the intralayer distances do change across the K*Ln*Se_2 series, Figure 1d. All bond lengths and atomic coordinates are listed in Tables S1−S2, and PXRD patterns of compounds can be found in Figures S1 and S2 in the Supporting Information.

Figure 1. (a) crystal structure of $KLaSe_2$. (b) Interlayer packing of La–La triangular lattice along *c*-axis. (c) $LaSe_6$-octahedra. (d) The change of unit cell volume of K*Ln*Se_2-series.

3.2. Magnetic Properties of K*Ln*Se₂. Temperature dependent magnetic susceptibilities were measured using 10 kOe applied magnetic field. Here, magnetic susceptibility was measured on single crystals with the applied magnetic field parallel and perpendicular to the *ab*-plane. Figure 2 displays the magnetic susceptibility of the Ce, Pr and Nd compounds between 2-300 K. The magnetic susceptibilities were fitted using the Curie-Weiss law, $\chi = C/(T-\theta_{CW})$, where χ is the susceptibility, C is the Currie constant, θ_{CW} is the Curie-Weiss temperature. Magnetic susceptibilities were fitted separately at high temperatures (150-300 K) and lower temperatures (2-10 K). The effective magnetic moment was calculated using μeff ~$2.828\sqrt{C}$ and the results are summarized in Table 2. Additionally, magnetic susceptibility of $KCeSe_2$ and $KNdSe_2$ was performed down to 0.4 mK. The isothermal magnetization was also performed at mK temperatures for both $KCeSe_2$ and $KNdSe_2$, Figure 3 and 4. Here, we only targeted the Kramer ions where the crystal electric field (CEF) can contribute to produce Kramers' doublet. A large magnetic anisotropy between *ab*-plane and *c*-axis magnetization was found in these compounds, revealing two-dimensional magnetism in these systems.

$KCeSe_2$. The magnetic susceptibility and inverse magnetic susceptibility (2-300 K) of $KCeSe_2$ are presented in Figure 2a. The susceptibility data was collected at the applied magnetic field of 1 T with the applied magnetic field parallel and perpendicular to the *ab*-plane. A strong magnetic anisotropy was observed between the two crystallographic orientations. The data parallel to the *c*-axis becomes very noisy at higher temperature due to the smaller magnetic signal. Therefore, we only fit the in-plane magnetic data of $KCeSe_2$. Here, the in-plane magnetic susceptibility at higher temperatures produces an effective magnetic moment, $\mu_{eff} = 2.47\ \mu_B$ and Curie-Weiss temperature of -35.8 K. Fitting the lower temperature region resulted an effective magnetic moment of $\mu_{eff} = 1.64\ \mu_B$ and Curie-Weiss temperature -2.41 K. This indicates an overall antiferromagnetic nature of the $KCeSe_2$. The magnetic susceptibility of $KCeSe_2$ from 1.6 to 0.4 K data is shown in Figure 3a. Magnetic susceptibility exhibits a broad transition at 0.8 K under 0.01 T and this could be due to the magnetic frustration. With increasing the applied magnetic field, the broad transition disappears at ~2 T by indicating a field induced magnetic transition. This is further confirmed from the isothermal magnetization data at 0.42 K where isothermal magnetization data exhibits a change in slope starting from 2 T and finally it reaches to a saturation at ~5 T with 1.0 μ_B/Ce.

$KPrSe_2$. Magnetic susceptibility of $KPrSe_2$, 2-300 K, is shown in Figure 2b, and high temperature (150-300 K) Curie-Weiss fitting yields, *H*//*ab*: θ_{CW} = -53.3 K, μ_{eff}/Pr = 2.75 μ_B and *H*//*c*: θ_{CW} = -118, μ_{eff}/Pr = 3.26 μ_B. These moments are very close to the calculated moment of free Pr^{3+} ($4f^2$, 3.58 μ_B). At lower temperatures, magnetic susceptibility deviates from Curie-Weiss law. A broad peak can be observed in both crystallographic directions between 50-25 K. Fitting the lower temperature (2-10 K) data resulted *H*//*ab*: θ_{CW} = -25.2 K, μ_{eff}/Pr = 2.21 μ_B and *H*//*c*: θ_{CW} = -10.9, μ_{eff}/Pr = 1.08 μ_B. These reduce moments can be attributed the crystal electric field. Isothermal magnetization of $KPrSe_2$ is given in the supporting information.

$KNdSe_2$. The temperature dependent magnetic susceptibility (2-300 K) of $KNdSe_2$ is depicted in Figure 2c. The high-temperature fitting values for *H*//*ab* and *H*//*c* are μ_{eff}/Nd = 3.72 μ_B, θ_{CW} = -22.5 K and μ_{eff}/Nd = 4.02 μ_B, θ_{CW} = -93.5 K , respectively. In contrast, lower temperature fitting yield μ_{eff}/Nd = 3.46 μ_B, θ_{CW} = -9.54 K and μ_{eff}/Nd = 2.48 μ_B, θ_{CW} = -1.70 K for *H*//*ab* and *H*//*c* respectively. The lower temperature moment is smaller compare to the free Nd^{3+} ions (μ_{eff} = 3.62 μ_B) and this could be due to the CEF where the ground state could break into Kramer's doublet. Similar behavior has been observed in previous Nd^{3+} containing frustrated magnetic lattices such as $NdZr_2O_7$ (2.54 μ_B/Nd^{3+}) [37] and $Nd_3SbZn_2O_{14}$ (2.3 μ_B/Nd^{3+}) [38] and $NdZnAl_{11}O_{19}$ (2.623 μ_B/Nd^{3+}) [39]. In addition, magnetic susceptibility of $KNdSe_2$ was measured down to 0.4 mK using applied magnetic fields between 0.1 and 7 T. No clear field induced magnetic transition was observed in $KNdSe_2$ with the applied magnetic field. As depicted in the isothermal magnetization data Nd-moment saturates along the *ab*-axis at around 2 T.

Table 2. Effective moments (μ_{eff}) and Curie-Weiss temperatures (θ_{CW}) determined by fitting inverse magnetic susceptibility data when the applied field parallel and perpendicular to the *ab*-plane for K*Ln*Se_2 series. These fitting were performed at high temperature (HT) regions (~300 K) and low temperature (LT) regions (~10 K).

		μ_{eff} (μB)	θ_{CW} (K) HT	μ_{eff} (μB)	θ_{CW} (K) LT
H//*ab*	$KCeSe_2$	2.47	-38.5	1.64	-2.41
	$KPrSe_2$	2.75	53.3	2.21	-25.2
	$KNdSe_2$	3.72	-22.5	3.46	-9.54
H//*c*	[illegible]	[illegible]	[illegible]	[illegible]	-10.9
	[illegible]	[illegible]	[illegible]	[illegible]	-1.70

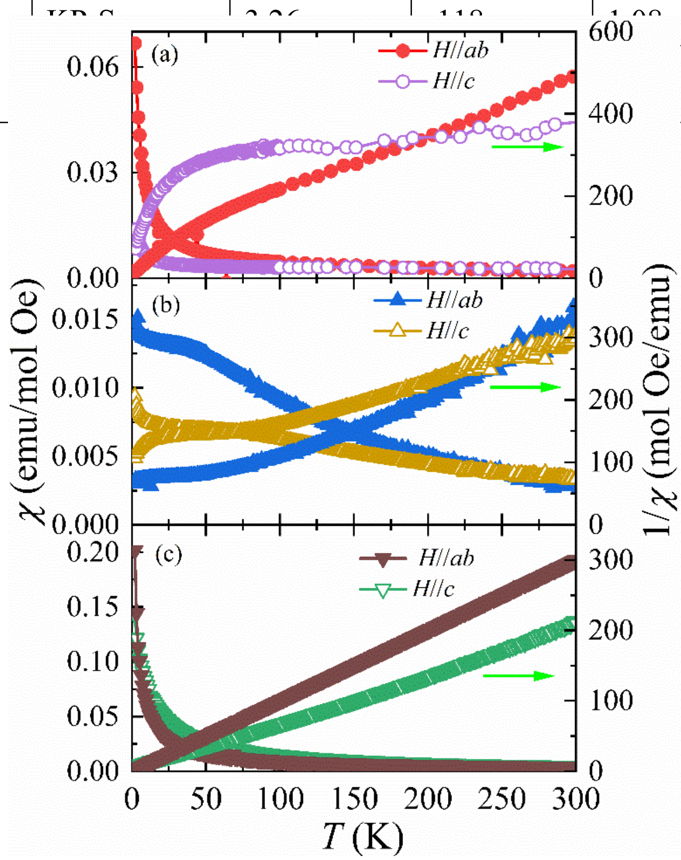

Figure 2. Magnetic susceptibility and inverse magnetic susceptibility of K*Ln*Se_2 series, (a) $KCeSe_2$; (b) $KPrSe_2$; (c) $KNdSe_2$, measured at applied magnetic field of 1 T in FC-mode. Each sample was measured with the applied magnetic field along the *ab*-plane and *c*-axis.

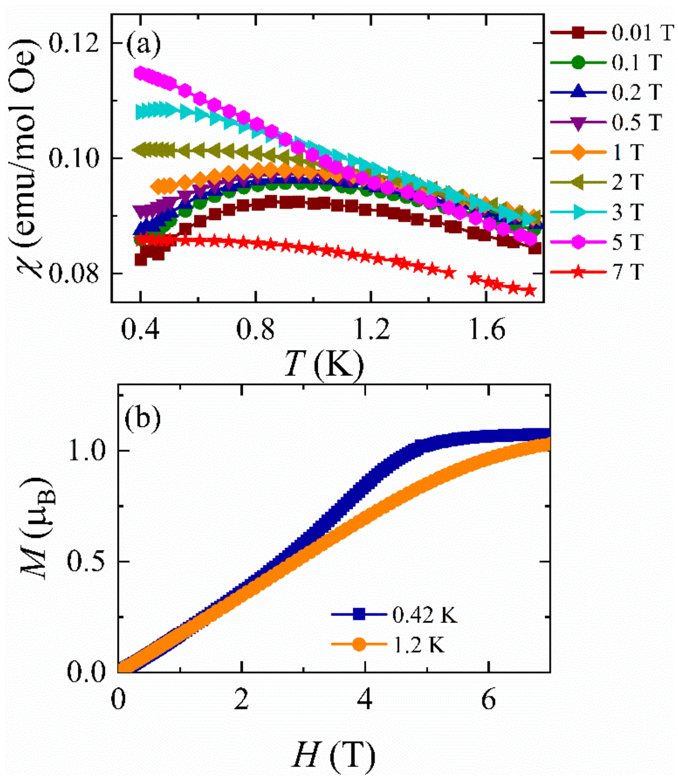

Figure 3. (a) Temperature dependence of *dc*-susceptibility for the $KCeSe_2$ single crystal in the *ab*-plane in different applied magnetic field. (b) Isothermal magnetization of $KCeSe_2$ along the *ab*-plane at mK temperatures.

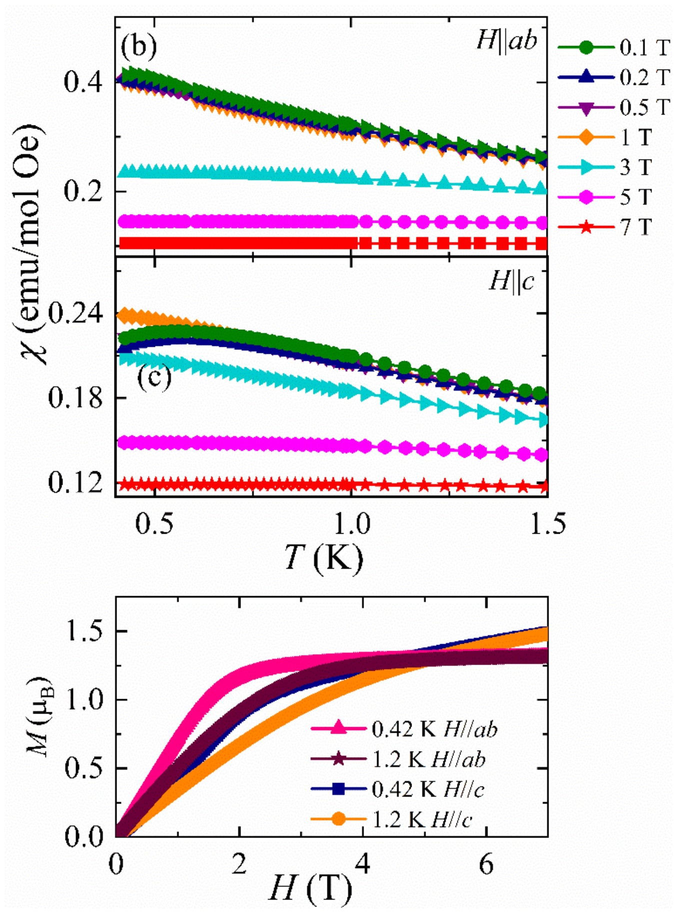

Figure 4. Temperature dependence of *dc*-susceptibility for the $KNdSe_2$ single crystal along the *ab*-plane (a) and *c*-axis (b) in different applied magnetic fields. (c) Isothermal magnetization of $KNdSe_2$.

The heat capacity of $KCeSe_2$ and $KNdSe_2$ were measured at zero applied magnetic field down to 0.4 mK, as shown in Figure 4 ($KPrSe_2$ was only measured down to 1.9 K). The magnetic heat capacity was estimated by subtracting the lattice contribution using the heat capacity of $KLaSe_2$. As depicted in Figure 5, no long-range order was found down to 0.4 K which agrees with our magnetic susceptibility data. Both $KCeSe_2$ and $KNdSe_2$ present a broad peaks at higher temperature suggesting short-range correlations. Figure 5 inset presents the temperature dependence of the entropy at 0 T for $KCeSe_2$ and $KNdSe_2$.

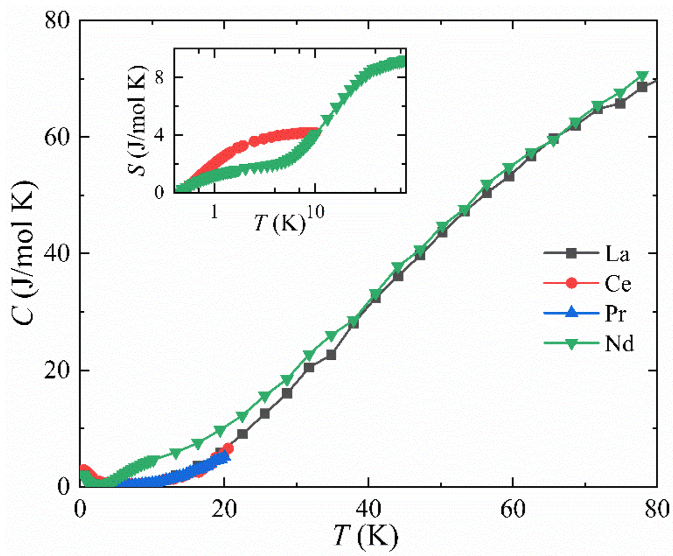

Figure 5. Temperature dependence of heat capacity of $KLnSe_2$ series down to 0.4 K. Inset: Temperature dependence of entropy at 0 T for $KCeSe_2$ and $KNdSe_2$.

3. CONCLUSION

The work here reports the single crystal synthesis and initial examination of the magnetic properties of $KLnSe_2$ (Ln = La, Ce, Pr, Nd). The reactions between K, Ln and Se elements were performed using a two-step flux growth method and yielded high purity good quality, often large single crystals. The $KLnSe_2$ series represents another addition to the collection of Delafossite 112-type crystal structures. The $KLnSe_2$ series crystallizes in trigonal crystal system with R-3m space group where the magnetic Ln^{3+} ions reside in ideal 2D triangular lattices which are separated by K^+-ions along the c-axis giving an ideal 2D nature to the structure. A magnetic investigation of $KLnSe_2$ indicates that all members studied here, have large magnetic anisotropies between the two crystallographic directions (ab-plane *vs.* c-axis). Magnetic susceptibilities reveal a dominant antiferromagnetic behavior and found no long-range ordering down to mK temperatures (0.4 mK). This work demonstrate that the salt flux is a viable method to synthesize this new family of compounds and while the analysis of magnetization data reveal both significant magnetic anisotropy and frustration in this series of compounds suggesting their potential for hosting interesting magnetic states.

CONFLICT OF INTEREST

There are no conflicts to declare.

ASSOCIATED CONTENT

Accession Codes

CCDC 2079221 and 2079222 contain the supplementary crystallographic data for this paper. These data can be obtained free of charge via www.ccdc.cam.ac.uk/data_request/cif, or by emailing data_request@ccdc.cam.ac.uk, or by contacting The Cambridge Crystallographic Data Centre, 12 Union Road, Cambridge CB2 1EZ, UK; fax: +44 1223 336033.

AUTHOR INFORMATION

Corresponding Author

Liurukara D Sanjeewa (sanjeewal@missouri.edu)

ORCID

Liurukara D. Sanjeewa: 0000-0002-3293-7370

Jie Xing: 0000-0002-9732-2318

Athena S. Sefat: 0000-0002-5596-3504

ACKNOWLEDGMENT

This research used resources at the Missouri University Research Reactor. The research at the Oak Ridge National Laboratory (ORNL) is supported by the U.S. Department of Energy (DOE), Office of Science, Basic Energy Sciences (BES), Materials Sciences and Engineering Division. This research used resources at the High Flux Isotope Reactor and Spallation Neutron Source, a DOE Office of Science User Facility operated by ORNL.

REFERENCES

[1] Lacroix, C.; Mendels, P.; Mila, F. *Introduction to Frustrated Magnetism: Materials, Experiments, Theory;* Springer Series in Solid State Sciences: Berlin: Springer, 2011.
[2] Giamarchi, T. *Quantum Physics in One Dimension;* Oxford University Press Inc.: New York, 2003.
[3] Taddei, K. M.; Sanjeewa, L. D.; Kolis, J. W.; Sefat, A. S.; de la Cruz, C.; Pajerowski, D. M. Local-Ising-Type Magnetic Order and Metamagnetism in the Rare-Earth Pyrogermanate $Er_2Ge_2O_7$. *Phys. Rev. Mater.* **2019**, *3*, 014405.
[4] Sanjeewa, L. D.; Ross, K. A.; Sarkis, C. L.; Nair, H. S.; McMillen, C. D.; Kolis, J. W. Single Crystals of Cubic Rare-Earth Pyrochlore Germanates: $RE_2Ge_2O_7$ (*RE* = Yb and Lu) Grown by a High-Temperature Hydrothermal Technique. *Inorg. Chem.* **2018**, *57*, 12456−12460.
[5] Natarajan, S.; Mandal, S. Open-Framework Structures of Transition-Metal Compounds. *Angew. Chem. Int. Ed.* **2008**, *47*, 4798−4828.
(6) Hwu, S.-J. Structurally Confined Transition-Metal Oxide Layers, Chains and Oligomers in Molecular and Extended Magnetic Solids. *Chem. Mater.* **1998**, *10*, 2846−2859.
[7] Krivovichev, S. V. Which Inorganic Structures are the Most Complex? *Angew. Chem. Int. Ed.* **2014**, *53*, 654−661.
[8] Bugaris, D. E.; zur Loye, H.-C. Materials Discovery by Flux Crystal Growth: Quaternary and Higher Order Oxides *Angew. Chem. Int. Ed.* **2012**, *51*, 3780 – 3811.
[9] Nguyen, L. T.; Cava, R. J. Hexagonal Perovskites as Quantum Materials. *Chem. Rev.* **2021**, *121*, 2935−2965.
[10] Moessner, R.; Ramirez, A. P. Geometrical Frustration, *Phys. Today* **2006**, *59*, 24–29.
[11] Anderson, P. W.; Resonating valence bonds: A New Kind of Insulator? *Mater. Res. Bull.* **1973**, *8*, 153–160.
[12] Mila, F. Quantum Spin Liquids, *Eur. J. Phys.* **2000**, *21*, 499–510.
[13] Balents, L. Spin Liquids in Frustrated Magnets, *Nature* **2010**, *464*, 199–208.
[14]. Gardner, J. S.; Gingras, M.; Greedan, J. E. Magnetic Pyrochlore Oxides, *Rev. Mod. Phys.* **2010**, *82*, 53–107.
[15]. Broholm, C.; Cava, R. J.; Kivelson, S. A.; Nocera, D. G.; Norman, M. R.; Senthil, T. Quantum Spin Liquids. *Science* **2020**, *367*, 263.
[16]. Li, Y.; Gegenwart, P.; Tsirlin, A. A. Spin Liquids in Geometrically Perfect Triangular Antiferromagnets, *J. Phys. Condens. Matter* **2020**, *32*, 224004.

[17] Sarkis, C. L.; Rau, J.G.; Sanjeewa, L. D.; Kolis, J. W.; Marbey, J.; Hill, S.; Rodriguez-Rivera, J. A.; Nair, H. S.; Gingras, M. J. P.; Ross K. A. Establishing Microscopic Interactions at a Phase Boundary: A Single Crystal Study of the Metastable Pyrochlore $Yb_2Ge_2O_7$, *Phy. Rev. B*, 2020, **102**, 134418.

[18]. Pajerowski, D. M.; Taddei, K. M.; Sanjeewa, L. D.; Savici, A. T.; Stone, M. B.; Kolis, J. W. Quantification of Local Ising Magnetism in Rare-Earth Pyrogermanates $Er_2Ge_2O_7$ and $Yb_2Ge_2O_7$. *Phys. Rev. B*, **2020**, *101*, 014420.

[19]. Wu L. S.; Nikitin, S. E.; Wang, Z.; Zhu, W.; Batista, C. D.; Tsvelik, A. M.; Samarakoon, A. M.; Tennant, D. A.; Brando, M.; Vasylechko, L.; Frontzek, M.; Savici, A. T.; Sala, G.; Ehlers, G.; Christianson, A. D.; Lumsden, M. D.; Podlesnyak, A.; Tomonaga-Luttinger Liquid Behavior and Spinon Confinement in $YbAlO_3$, *Nat. Commun.* **2019**, *10*, 698.

[20] Garlea, V. O.; Sanjeewa, L. D.; McGuire, M. A.; Batista, C. D.; Samarakoon, A. M.; Graf, D.; Winn, B.; Ye, F.; Hoffmann, C.; Kolis, J. W. Exotic Magnetic Field-Induced Spin-Superstructures in a Mixed Honeycomb-Triangular Lattice System. *Phys. Rev. X* **2019**, *9*, 011038.

[21] Xing, J.; Taddei, K. M.; Sanjeewa, L. D.; Fishman, R. S.; Daum, M.; Mourigal, M.; dela Cruz, C.; Sefat, S. A. Stripe Antiferromagnetic Ground State of Ideal Triangular Lattice $KErSe_2$. *Phy. Rev. B* **2021**, *103*, 144413.

[22] Scheie, A.; Garlea, V. O.; Sanjeewa, L. D.; Xing, J.; Sefat, A. S. Crystal-field Hamiltonian and Anisotropy in $KErSe_2$ and $CsErSe_2$. *Phys. Rev. B* **2020**, *101*, 144432.

[23] Ferreira, T.; Xing, J.; Sanjeewa, L. D.; Sefat, A. S. Frustrated Magnetism in Triangular Lattice $TlYbS_2$ Crystals Grown via Molten Flux. *Front. Chem.* **2020**, *8*, 127.

[24] Xing, J.; Sanjeewa, L. D.; Kim, J.; Stewart, G. R.; Du, M.-H.; Reboredo, F. A.; Custelcean, R.; Sefat, A. Crystal Synthesis and Frustrated Magnetism in Triangular Lattice Cs*RE*Se_2 (*RE* = La–Lu): Quantum Spin Liquid Candidates $CsCeSe_2$ and $CsYbSe_2$. *ACS Materials Lett.* **2020**, *2*, 71−75.

[25] Xing, J.; Sanjeewa, L. D.; Kim, J.; Stewart, G. R.; Podlesnyak, A.; Sefat, A. S. Field-induced Magnetic Transition and Spin Fluctuation in Quantum Spin Liquid Candidate $CsYbSe_2$. *Phys. Rev. B* **2019**, *100*, 220407(R).

[26] Xing, J.; Sanjeewa, L. D.; Kim, J.; Meier, W. R.; May, A. F.; Zheng, Q.; Custelcean, R.; Stewart, G. R.; Sefat, A. S. Synthesis, Magnetization, and Heat Capacity of Triangular Lattice Materials $NaErSe_2$ and $KErSe_2$. *Phys. Rev. M* **2019**, *3*, 114413.

[27] Bastien, G.; Rubrecht, B.; Haeussler, E.; Schlender, P.; Zangeneh, Z.; Avdoshenko, S.; Sarkar, R.; Alfonsov, A.; Luther, S.; Onykiienko, A.; Walker, H. C.; Kühne, H.; Grinenko. V.; Guguchia, Z.; Kataev, V.; Klauss, H.; Hozoi, L.; Brink, J.; Inosov, D. S.; Büchner, B.; Wolter, A. U. B.; Doert, T. Long-range Magnetic Order in the S = 1/2 Triangular Lattice Antiferromagnet $KCeS_2$. *SciPost Phys.* **2020**, *9*, 041.

[28] Bordelon, M. M.; Wang, X.; Pajerowski, D. M.; Banerjee, A.; Sherwin, M.; Brown, C. M.; Eldeeb, M. S.; Petersen, T.; Hozoi, L.; Rößler, U. K.; Mourigal, M.; Wilson, S. D. Magnetic Properties and Signatures of Moment Ordering in the Triangular Lattice Antiferromagnet $KCeO_2$. *Phys Rev B* **2021**, *104*, 094421.

[29] Li, Y.; Chen, G.; Tong, W.; Pi, L.; Liu, J.; Yang, Z.; Wang, X.; Zhang, Q. Rare-earth Triangular Lattice Spin Liquid: A Single-crystal Study of $YbMgGaO_4$. *Phys. Rev. Lett.* **2015**, *115*, 167203.

[30] Li, Y.; Adroja, D.; Biswas, P. K.; Baker, P. J.; Zhang, Q.; Liu, J.; Tsirlin, A. A.; Gegenwart, P.; Zhang, Q, Muon Spin Relaxation Evidence for the U(1) Quantum Spin-Liquid Ground State in the Triangular Antiferromagnet $YbMgGaO_4$. *Phys. Rev. Lett.* **2016**, *117*, 097201.
[31] Bordelon, M. M.; Kenney, E.; Liu, C.; Hogan, T.; Posthuma, L.; Kavand, M.; Lyu, Y.; Sherwin, M.; Brown, C.; Graf, M.; Balents, L.; Wilson, S. D.; Field-tunable Quantum Disordered Ground State in the Triangular Lattice Antiferromagnet $NaYbO_2$. *Nat. Phys.* **2019**, *15*, 1058–1064.
[32] Baenitz, M.; Schlender, P.; Sichelschmidt, J.; Onykiienko, Y. A.; Zangeneh, Z.; Ranjith, K. M.; Sarkar, R.; Hozoi, L.; Walker, H. C.; Orain, J. C.; Yasuoka, H.; Brink, J.; Klauss, H. H.; Inosov, D. S.; Doert, T. $NaYbS_2$: A Planar Spin-1/2 Triangular-lattice Magnet and Putative Spin Liquid. *Phys. Rev. B* **2018**, *98*, 220409.

[33] Xie, T.; Xing,J.; Nikitin, S. E.; Nishimoto, S.; Brando, S.; Khanenko, P.; Sichelschmidt, J.; Sanjeewa, L. D.; Sefat, A. S.; Podlesnyak, A.; Field-Induced Spin Excitations in the Spin-1/2 Triangular-Lattice Antiferromagnet $CsYbSe_2$. (*https://arxiv.org/pdf/1911.12286*).
[34] $CsCeSe_2$-manuscript under preparation.
[35] *Apex3*, Bruker AXS Inc., Madison, WI, **2015.**
[36] G. M Sheldrick, Crystal structure refinement with SHELXL, Acta Crystallographica Section C: Structural Chemistry, **2015**, *71* ,3–8
[37] Xu, J.; Anand, V. K.; Bera, A. K.; Frontzek, M.; Abernathy, D. L.; Casati, N.; Siemensmeyer, K.; Lake, B. Magnetic Structure and Crystal-field States of the Pyrochlore Antiferromagnet $NdZr_2O_7$. *Phys. Rev. B* **2015**, *9*, 224430.
[38] Sanders, M. B.; Krizan, W.; Cava, R. J. $RE_3Sb_3Zn_2O_{14}$ (*RE* = La, Pr, Nd, Sm, Eu, Gd): A New Family of Pyrochlore Derivatives with Rare Earth Ions on a 2D Kagome Lattice. *J. Mater. Chem. C*. **2016**, 4, 541–550.
[39] Ashtar, M.; Marwat, M. A.; Gao, X. Y.; Zhang, Z. T.; Pi, L.; Yuana, S. L.; Tian, Z. M. $REZnAl_{11}O_{19}$ (*RE* = Pr, Nd, Sm–Tb): a New Family of Ideal 2D Triangular Lattice Frustrated Magnets. *J. Mater. Chem. C* **2019**, *7*, 10073–10081.

For Table of Contents Use Only:

Synthesis, Crystal Structure and Magnetic Properties of KLnSe2 (Ln = La, Ce, Pr, Nd) Structures: A family of 2D Triangular Lattice Frustrated Magnets

Liurukara D. Sanjeewa, Jie Xing, Keith M. Taddei, Athena S. Sefat

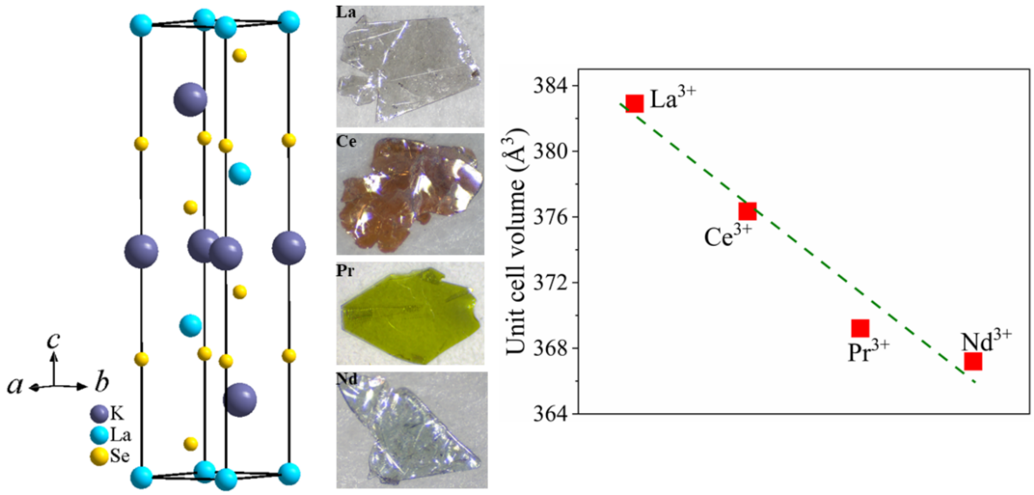

Four new Delafossite 112-type crystal structures, K*Ln*Se_2 (*Ln* = La, Ce, Pr, Nd) series have been successfully synthesized and characterized. The newly designed flux growth method resulted large disorder free single crystals. The structures are characterized by a geometrically frustrated Ln-triangular lattice. The magnetic measurement revealed that K*Ln*Se_2 (*Ln* = Ce, Pr, Nd) do not show any long-range ordering down to 0.4 mK.